Rapid thermal processing for fast sintering of Mn–Cu spinel coatings deposited by electrophoretic deposition

Ceramics International xxx (xxxx) xxx

Contents lists available at ScienceDirect

Ceramics International

journal homepage: www.elsevier.com/locate/ceramint

Rapid thermal processing for fast sintering of Mn–Cu spinel coatings deposited by electrophoretic deposition

Francesco Gallo [a,*], Marc Torrell [b], Lucile Bernadet [b], Simone Anelli [a], Fabiana D'Isanto [a], Dario Montinaro [c], Federico Smeacetto [a]

[a] Department of Applied Science and Technology, Politecnico di Torino, Corso Duca Degli Abruzzi 24, Torino, 10129, Italy
[b] IREC, Catalonia Institute for Energy Research, Dept of Advanced Materials for Energy Applications, Jardins de les Dones de Negre 1, Sant Adrià Del Besòs, Barcelona, 08930, Spain
[c] SolydEra SpA, Viale Trento 117, Mezzolombardo, 38017, Italy

ARTICLE INFO

Keywords:
Electrophoretic deposition
Solid oxide cells
Rapid thermal processing
Protective coatings

ABSTRACT

Compact Mn–Cu spinel protective coatings were fabricated on AISI 441 ferritic stainless steel by electrophoretic deposition (EPD) followed by rapid thermal processing (RTP). The proposed approach enabled the formation of compact, adherent and partially densified coatings within significantly reduced processing times (below 1 h). A processing window was identified by varying RTP temperature and dwell time, highlighting the strong influence of thermal parameters on coating densification and adhesion. In situ high-temperature X-ray diffraction (HT-XRD) analysis of the Mn–Cu spinel powder revealed phase evolution during heating, including the growth of CuO-related peaks and spinel instability at 950 °C. Microstructural characterization showed that RTP conditions strongly affect coating morphology, densification behaviour, and thickness uniformity. Crack-free coatings were obtained under optimized conditions, while EDS analysis showed no detectable chromia scale formation at the coating/substrate interface after RTP treatment. The results demonstrate that RTP-assisted EPD is a promising and potentially scalable route for the fabrication of Mn–Cu spinel protective coatings for SOC interconnects, enabling rapid densification while limiting thermal exposure and interfacial degradation phenomena.

1. Introduction

Interconnects play a critical role in solid oxide cells (SOCs), acting as both electrical connectors between adjacent cells and physical barriers separating the fuel and oxidant gases. In addition, they ensure current collection and distribution across the stack while maintaining structural integrity under high-temperature operating conditions [1,2]. Interconnects represent one of the most cost-intensive components in SOC stacks, accounting for a significant fraction (approximately 11–15%) of the total system cost [3] and contributing substantially to the overall stack weight [4].

While specialized alloys such as Crofer-type steels offer improved oxidation resistance and long-term stability, their cost has been reported to be up to one order of magnitude higher than that of commercially available ferritic stainless steels [3], limiting their large-scale deployment [4]. In contrast, commercially available ferritic stainless steels, such as AISI 441, provide a cost-effective alternative, combining adequate electrical conductivity, good thermo-mechanical compatibility, and ease of manufacturing [5–7].

However, under typical SOC operating conditions (600–850 °C), these materials are prone to degradation due to high-temperature oxidation and chromium volatilization [1]. The growth of the chromia scale on the steel surface leads to an increase in electrical resistance [8], while the formation and transport of volatile chromium species can result in cathode poisoning and severe performance losses [9,10]. For this reason, the application of protective coatings is essential to enhance interconnect durability by limiting chromia scale growth, suppressing chromium evaporation, and improving the overall electrochemical stability of the system [6,11,12].

Electrophoretic deposition (EPD) has emerged as a highly attractive technique for fabricating protective spinel coatings on SOC interconnects. Compared to other state-of-the-art deposition techniques (e.g. sol-gel dip-coating [13–15], screen printing and slurry coating [4,16], radio frequency (rf) magnetron sputtering [17,18], pulsed laser deposition [19–21], plasma spraying [22,23]) EPD is characterized by simplicity, low cost, scalability, and the ability to uniformly coat

* Corresponding author.
E-mail address: francesco.gallo@polito.it (F. Gallo).

https://doi.org/10.1016/j.ceramint.2026.08.190
Received 10 June 2026; Received in revised form 28 July 2026; Accepted 13 August 2026
Available online 13 August 2026

complex geometries [24,25]. This aspect is particularly relevant for SOC interconnects, which typically feature three-dimensional architectures with flow channels designed for gas distribution. Achieving a homogeneous coating over such non-planar and structured surfaces is essential to ensure uniform protection and electrical performance across the entire component [26,27]. In addition, EPD allows precise control of coating thickness and morphology via simple adjustment of deposition parameters, while maintaining low material consumption [2,28,29]. However, a key limitation of EPD is the requirement of post-deposition sintering, as the as-deposited layer consists of loosely packed particles that must be densified to achieve adequate mechanical stability [30,31].

Among protective coating materials, manganese–cobalt (Mn-Co) spinels are currently considered the state-of-the-art due to their high electrical conductivity, good thermal expansion compatibility, and effective chromium blocking capability [11,32–41]. On the other hand, cobalt-containing materials are associated with higher cost and potential environmental and health concerns related to the extraction and processing of cobalt resources [42,43]. Therefore, increasing attention is being devoted to alternative compositions, particularly manganese–copper (Mn–Cu) spinels, driven by both economic and environmental considerations [44–51]. In this context, Mn–Cu spinels represent a promising alternative, offering comparable or even higher electrical conductivity and suitable thermo-mechanical compatibility with ferritic stainless steels, while reducing reliance on critical raw materials [47,52,53]. Despite these advantages, Mn–Cu systems have been less extensively investigated than Mn-Co spinels.

Despite the promising properties of these spinel coatings, achieving a dense, well-adherent layer after deposition remains one of the most critical challenges. In fact, conventional sintering treatments, which typically involve prolonged high-temperature exposure in industrial furnaces or reduction–reoxidation cycles, can promote chromia scale formation at the steel/coating interface while increasing processing time and cost [8,54,55]. Such effects are particularly critical in SOCs applications, where interfacial reactions and scale growth strongly influence long-term performance [1,8,12,55]. Traditional thermal treatments are often inherently energy-intensive and contribute significantly to manufacturing costs, due to both the high-power demand required to maintain elevated temperatures and the associated capital and operational expenses of high-temperature equipment. Indeed, sintering-based manufacturing processes are recognized as major contributors to energy consumption in industrial sectors, while furnace complexity and operating conditions can substantially increase production costs [2,28,29]. Moreover, prolonged exposure to high temperatures increases environmental impact through increased energy use and emissions [29].

Alternative deposition techniques that enable direct formation of dense coatings without post-sintering, such as plasma spraying, have been explored to overcome these limitations. These approaches can produce dense layers during deposition and limit chromia scale growth at the interface [22,23]. However, they typically involve higher process complexity, increased energy demand, and lower powder utilization efficiency compared to suspension-based techniques [29]. To overcome the limitations associated with conventional sintering, a wide range of rapid sintering techniques has been developed in recent years, aiming to reduce processing time, thermal budget, and grain coarsening while improving densification efficiency [56–60]. Among these approaches, field-assisted sintering techniques (FAST), including spark plasma sintering (SPS) and flash sintering, have attracted considerable attention due to their extremely high heating rates (up to 10^2 –10^4 °C·min^{-1}) and the possibility of achieving densification within seconds [56–59]. Similarly, microwave sintering enables volumetric and rapid heating by direct interaction between electromagnetic radiation and the material, reducing thermal gradients and processing times [60]. More recently, emerging techniques such as ultrafast high-temperature sintering (UHS) and photonic or laser-based methods have demonstrated ultra-short processing times, often in the order of seconds, although they are still limited by scalability and process complexity [61,62]. Despite these advances, many of these techniques require specific sample geometries, electrical contact, or complex equipment, which may limit their applicability to coating systems and industrial-scale processes. As a result, rapid thermal processing (RTP) has emerged as a promising alternative [63–65]. RTP is a non-contact thermal treatment technique based on radiative heating (typically using halogen lamps), capable of achieving very high heating and cooling rates, with temperature ramps from room temperature to several hundred or thousands of degrees within seconds [64]. Compared to other rapid sintering methods, RTP combines fast thermal cycles with relatively simple equipment and good compatibility with planar substrates, making it particularly attractive for thin-film and coating processing. Moreover, the short dwell times and reduced thermal exposure can limit undesired diffusion, phase transformations, and interfacial reactions [66]. Building on these features, the combination of EPD and RTP represents a promising strategy to drastically reduce thermal exposure time, enabling rapid densification while preserving the advantages of a scalable and low-cost deposition technique. Nevertheless, the application of RTP to densify EPD-derived spinel coatings for SOC interconnect protection has not yet been explored.

In this work, Mn–Cu spinel coatings are deposited by EPD on AISI 441 ferritic stainless steel and subsequently densified by RTP. Unlike conventional sintering approaches, the proposed methodology enables the formation of compact and adherent coatings within significantly reduced processing times (below 1 h), while limiting thermal exposure and effectively reducing chromia scale formation at the coating/substrate interface during processing. This study provides the first systematic investigation of the combined use of EPD and RTP for Mn–Cu spinel coatings in SOC interconnect applications, highlighting the critical role of fast thermal cycles in controlling densification kinetics, phase stability, and interfacial phenomena. By decoupling densification from prolonged high-temperature exposure, the RTP approach offers a viable pathway to overcome the intrinsic limitations of conventional sintering.

Overall, this strategy establishes a time- and energy-efficient route for the fabrication of Mn–Cu-based protective coatings, while simultaneously addressing key degradation mechanisms associated with elemental interdiffusion, thus opening new perspectives for the industrial implementation of cost-effective spinel coated SOC interconnects.

2. Experimental

2.1. Samples preparation

A manganese–copper spinel coating was deposited by EPD onto AISI 441 ferritic stainless-steel substrates (Thyssen Krupp). According to the supplier datasheet, the nominal chemical composition of AISI 441 (wt%) is: Cr 17.5–18.5, C $\leq$ 0.03, Mn $\leq$ 1.0, Si $\leq$ 1.0, Ti 0.10–0.60, P $\leq$ 0.040, S $\leq$ 0.015, Nb (3×C + 0.30)–1.00, Fe balance [67].

Prior to deposition, the substrates (10 mm × 10 mm × 0.2 mm) were ultrasonically cleaned (SONICA® 3300 (9.5lt) EP S3) in acetone (Merck KGaA) and ethanol (Merck KGaA) for 10 min.

Commercially available Mn1.7Cu1.3O4 spinel powder was supplied by SolydEra and used as received. The powder had a median particle size of d_{50} = 1.28 μm. A suspension containing 10 g L^{-1} of spinel powder was prepared in a 50:50 vol% ethanol–acetone mixture. Iodine (Merck KGaA) (1 g L^{-1}) was added as a charging agent to increase the electrophoretic mobility of the particles [68].

A two-electrode configuration was used for the EPD process, with the substrate acting as the working electrode and a counter electrode placed at an interelectrode distance of 10 mm. A constant voltage of 15 V was applied for 90 s (Power Supply EV Series EV3620 Carl Roth).

The EPD parameters were selected based on previous optimization activities performed with the same Mn–Cu spinel suspension and conventional thermal treatments, as well as on literature reports on EPD of Mn–Cu spinel coatings for SOC interconnect applications. Since the present work focuses on the RTP post-deposition treatment, the EPD conditions were deliberately chosen to obtain a continuous, relatively thin green coating to minimize cracking or delamination during the initial RTP optimization. Therefore, these parameters should be considered a suitable starting point for assessing the feasibility of RTP-assisted sintering, rather than fully optimized conditions for achieving the final target coating thickness. Future work will focus on optimizing the EPD step to increase coating thickness while preserving adhesion and coating integrity.

2.2. Sintering of the coated samples

After deposition, the rapid evaporation of the organic solvents allowed direct thermal treatment without additional drying steps. The thermal treatment was carried out using a rapid thermal processing system (AS-One 100, Annealsys), shown in Fig. 1a, in which tungsten–halogen lamps provide rapid heating within a controlled-atmosphere chamber. During the treatment, air was continuously introduced into the chamber at a flow rate of 150 sccm, while the chamber pressure was maintained at 250 mbar.

The process is schematically illustrated in Fig. 1b, while Fig. 1c compares the processing time required for conventional sintering, as reported in Ref. [69], with that of the RTP approach.

A processing window was investigated to identify the temperature and time conditions that yield partially densified, crack-free coatings. Based on this optimization, three sets of parameters were selected: 850 °C for 15 min, 875 °C for 10 min, and 900 °C for 1 min. The corresponding samples were labelled MnCu_850_15, MnCu_875_10, and MnCu_900_1. A heating rate of 50 °C s^{-1} was applied, while cooling occurred primarily by thermal inertia, reaching 150 °C in approximately 10 min. A thermocouple was used to monitor the sample temperature during the treatment.

For each selected RTP condition, two independently prepared samples were processed to verify the consistency of coating adhesion, visual integrity, and microstructural features. The reported processing window should thus be considered as an initial RTP optimization, while a broader statistical reproducibility assessment will be addressed in future work.

2.3. Characterization

Particle size distribution of the starting powder was evaluated by laser diffraction (Mastersizer 3000, Malvern Panalytical). The phase composition of the as-received powder and thermally treated samples was determined by X-ray diffraction (XRD; PANalytical Empyrean) using Cu Kα radiation in the 2θ range of 20–70°, with a step size of 0.013° and a counting time of 100 s per step. Phase identification was performed using HighScore software and the ICDD (International Centre for Diffraction Data, Newtown Square, PA, USA) database. In situ high-temperature X-ray diffraction (HT-XRD) was conducted using the same diffractometer equipped with a high-temperature chamber (Anton Paar HTK1200N) to investigate phase evolution during heating in air. Measurements were collected at 25 °C, then every 50 °C from 600 °C to 950 °C, and finally after cooling to room temperature at the end of the thermal cycle. A dwell time of 10 min was applied prior to each measurement to ensure thermal stabilization, and a heating rate of 3 °C min^{-1} was used. Morphological analysis of the surface and cross-sections of the sintered coatings was performed using field-emission scanning electron microscopy (FE-SEM; MIRA3, TESCAN). Elemental composition and mapping were obtained by energy-dispersive X-ray spectroscopy (EDS) using FE-SEM instruments (SUPRA™ 40 and Merlin Gemini, Zeiss; MIRA3 XMH, TESCAN). For cross-sectional observations, samples were embedded in epoxy resin (Struers, Denmark), ground using SiC papers up to 4000 grits, polished with diamond suspensions, and finally sputter-coated with Pt. The porosity of the coatings was estimated from cross-sectional SEM images using ImageJ software (NIH, USA) by image thresholding and area fraction analysis. To assess the reproducibility of the EPD step, three independently deposited green coatings were prepared under the selected EPD conditions and the deposited mass was measured by weighing the substrates before and after deposition. In addition, the surface roughness of representative green coatings was measured by confocal microscopy (LSM900 Zeiss) and compared with that of the bare AISI 441 substrate.

3. Results

3.1. Phase evolution of Mn–Cu spinel during thermal treatment

In situ HT-XRD analysis was performed to investigate the phase evolution of the Mn–Cu spinel powder during thermal treatment and to identify the temperature range relevant for RTP processing. The results, summarized in Fig. 2, show that significant changes in the diffraction pattern occur at 950 °C, in agreement with the phase diagram [52], indicating that this temperature corresponds to a critical region for spinel stability under conventional heating conditions [70].

Below this temperature, no complete phase decomposition is observed; however, progressive modifications of the diffraction patterns indicate the onset of phase evolution during heating. In particular, an increase in the intensity of peaks associated with copper oxide (CuO) is detected with increasing temperature. This behaviour suggests a redistribution of copper within the system and the formation of secondary phases during thermal treatment. The evolution of secondary phases within the coating system may affect the thermo-mechanical compatibility of the material, since phases with different properties can

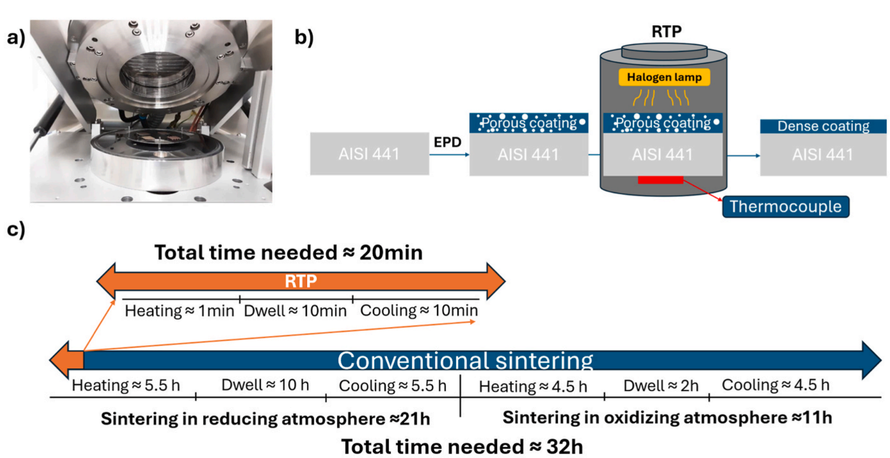

Fig. 1. a) RTP system AS-One 100, Annealsys b) Schematic representation of the RTP process c) Sintering time comparison between RTP and conventional sintering.

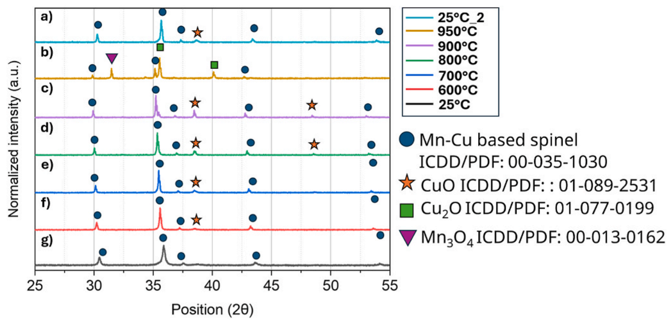

Fig. 2. X-ray diffraction patterns of Mn–Cu spinel powder at different temperatures a) 25 °C after cooling b) 950 °C c) 900 °C d) 800 °C e) 700 °C f) 600 °C g) 25 °C.

introduce local thermal expansion mismatch and internal stresses, potentially leading to microstructural degradation and reduced coating stability [71–73]. In addition, a systematic shift of the diffraction peaks toward lower angles is observed with increasing temperature, consistent with thermal lattice expansion according to Bragg's law.

After cooling to room temperature at the end of the thermal cycle, the diffraction pattern shows the reappearance of the spinel-related peaks, indicating partial recovery of the spinel structure. However, CuO-related peaks remain detectable after cooling, suggesting that the phase evolution occurring during heating is only partially reversible.

These results provide useful information for defining the thermal limits of the RTP process. In particular, the phase evolution observed close to 950 °C indicates that this temperature range should be avoided, even under rapid thermal cycles, as transient phase changes may generate local thermo-mechanical mismatch and contribute to stress development within the coating. Therefore, the HT-XRD analysis was used as a reference to guide the selection of RTP conditions below this critical temperature range.

In conventional sintering, temperatures in the range of 850–900 °C are commonly employed to achieve sufficient densification of spinel coatings [11,35,45,74–77]. However, when combined with prolonged dwell times, such conditions may promote phase evolution and interfacial reactions such as interdiffusion and chromia scale formation within the coating/substrate system [55,78]. For this reason, RTP treatments were investigated in the same temperature interval, aiming to promote coating densification while strongly reducing the duration of thermal exposure.

3.2. RTP processing window

Based on the thermal behaviour identified by HT-XRD, RTP temperature and dwell time were systematically varied to determine a processing window suitable for coating densification without compromising adhesion and integrity. The resulting processing window, summarized in Fig. 3, was defined based on microstructural observations

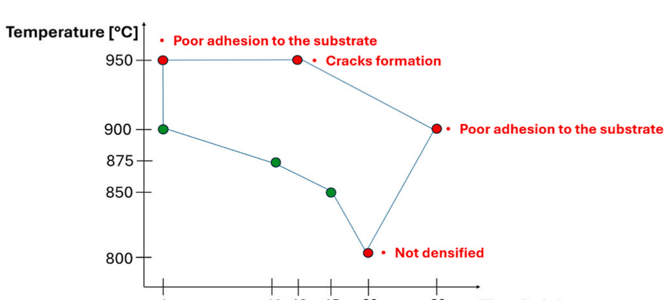

Fig. 3. Processing window for RTP conditions showing coating quality as a function of temperature and dwell time.

and adhesion behaviour, while only the most relevant conditions are reported.

A treatment at 800 °C for 20 min was insufficient to ensure adequate coating adhesion, indicating that densification was limited under these conditions. In contrast, treatments at 950 °C resulted in severe thermal stresses, leading to cracking and/or delamination. This behaviour is consistent with the HT-XRD results, which identified 950 °C as a critical temperature region for phase evolution of the Mn–Cu spinel system. Similarly, prolonged exposure at 900 °C (30 min) resulted in poor adhesion, suggesting that excessive thermal input promotes degradation at the coating/substrate interface. Optimal conditions were identified as 850 °C for 15 min, 875 °C for 10 min, and 900 °C for 1 min, yielding crack-free coatings with good adhesion. These results highlight a relatively narrow processing window, requiring a precise balance between temperature and dwell time to achieve defect-free coatings. Due to the rapid heating and cooling rates associated with RTP, relatively small variations in temperature and dwell time may result in significantly different thermal histories and densification behaviours [63,64]. This is consistent with the results obtained in the present work, where minor changes in the RTP parameters led to marked differences in coating densification and adhesion.

The identified processing window demonstrates that RTP enables effective densification under reduced thermal exposure, provided that the thermal input is carefully controlled to avoid insufficient consolidation at low temperature and adhesion loss or cracking at excessive temperature or dwell time. In this framework, the selected conditions of 850 °C for 15 min, 875 °C for 10 min, and 900 °C for 1 min represent the most promising RTP treatments for further microstructural and compositional analysis.

3.3. Phase composition of RTP-treated coatings

The XRD patterns of the RTP-treated coatings are reported in Fig. 4 together with the diffraction pattern of the as-received Mn–Cu powder. The analysis was carried out to evaluate the phase composition of the coatings after RTP treatment and to verify whether the selected processing conditions preserved the spinel structure in the final coating after cooling. All investigated samples exhibit the characteristic diffraction peaks of the spinel structure, indicating that the spinel phase remains the predominant crystalline phase after RTP treatment within the investigated processing window.

Nonetheless, differences in the evolution of CuO-related peaks are observed depending on the applied thermal treatment. In particular, the CuO-related peak appears more pronounced in the MnCu_850_15 sample compared to MnCu_875_10 and MnCu_900_1, despite the lower treatment temperature. This behaviour suggests that dwell time plays a major role in copper redistribution and secondary phase evolution during RTP treatment. Although higher temperatures are reached in MnCu_875_10

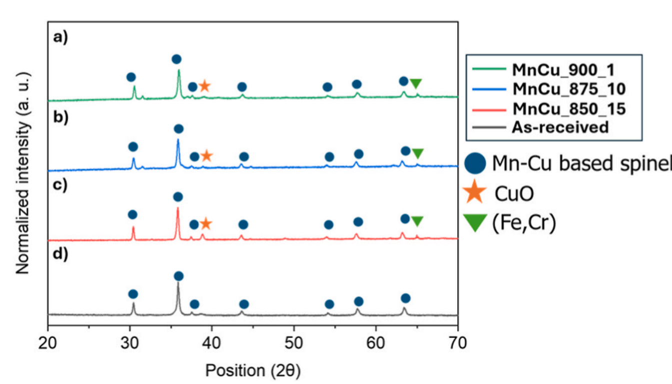

Fig. 4. X-ray diffraction patterns of thermally treated samples compared with the as-received Mn–Cu powder a) MnCu_900_1 b) MnCu_875_10 c) MnCu_850_15 d) Powder as-received.

and MnCu_900_1, the significantly shorter thermal exposure appears to limit the extent of Cu diffusion and associated CuO formation. These observations indicate that, within the selected RTP window, phase evolution in the final coating is influenced not only by peak temperature but also by the duration of thermal exposure. In particular, longer dwell times appear to favour copper redistribution and secondary phase stabilization even at comparatively lower temperatures. This result supports the need to optimize both temperature and dwell time rather than considering temperature alone.

Additionally, a peak at around 65.1° appears after sintering and can be attributed to Fe–Cr phases originating from the substrate. The presence of this signal suggests that the coating thickness is limited, allowing a partial contribution from the underlying substrate to the diffraction pattern.

The XRD results therefore indicate that the selected RTP treatments maintain the spinel phase as the main crystalline phase in the final coatings, while differences in CuO-related peak intensity highlight the role of dwell time in secondary phase evolution. These findings provide the basis for the subsequent microstructural and elemental analysis of MnCu_850_15, MnCu_875_10, and MnCu_900_1.

3.4. Microstructural evolution and densification behaviour

The microstructural evolution of the RTP-treated coatings was investigated by FE-SEM, as shown in Fig. 5. Top-view images (Fig. 5a–c) reveal crack-free surfaces for all selected RTP conditions, confirming that the identified processing window enables coating densification without surface cracking. However, clear differences in particle arrangement and aggregation are observed depending on the applied thermal treatment.

In MnCu_850_15, the particles appear well sintered but relatively loosely aggregated, suggesting that grain growth has occurred without extensive coalescence between neighbouring particles. In MnCu_875_10, particles exhibit similar sizes but appear more strongly aggregated, indicating enhanced inter-particle bonding and a more advanced stage of densification. In contrast, MnCu_900_1 shows a less uniform particle size distribution, with smaller grains that appear more densely packed and aggregated, suggesting a rapid densification process accompanied by less controlled microstructural evolution.

Cross-sectional observations (Fig. 5d–f) further support these trends. In all cases, the coatings exhibit predominantly closed porosity, indicating that the densification process is sufficiently advanced to isolate pores within the microstructure. However, clear differences in thickness distribution are observed. The MnCu_850_15 sample exhibits a more uniform coating thickness along the substrate, while MnCu_875_10 and MnCu_900_1 show more noticeable thickness variations, indicating a less homogeneous redistribution of material during sintering.

Coating thickness and porosity values were determined from the cross-sectional SEM images reported in Fig. 5 and are summarized in Table 1. The MnCu_850_15 sample exhibits the highest thickness (7.6 ± 0.5 μm) and a porosity of 24.8%, while MnCu_875_10 and MnCu_900_1 show reduced thickness (~4–5 μm) with comparable porosity values of 21.0% and 22.7%, respectively.

The reproducibility of the EPD step was evaluated by measuring the deposited mass on three independently prepared green coatings. The deposited masses were 2.4, 2.5, and 2.3 mg on 1.5 cm × 1.5 cm substrates, corresponding to 1.07 ± 0.04 mg cm^{-2} and to a coefficient of variation of approximately 4.2%. This result supports the reproducibility of the EPD process under the selected conditions. Confocal microscopy of representative green coatings revealed sub-micrometric surface roughness, with an average Sa of 0.47 ± 0.13 μm, compared with Sa = 0.192 μm for the bare AISI 441 substrate, indicating a relatively homogeneous surface morphology prior to RTP. Therefore, although minor local variations in the initial coating cannot be mainly ruled out, and the differences observed after RTP are primarily discussed in relation to the applied thermal treatment.

Although the measured porosity values exceed 20%, cross-sectional SEM observations suggest that the residual porosity is mainly isolated/closed rather than forming continuous open pathways through the

Table 1
Coating thickness values (mean ± SD) and porosity determined from cross-sectional Fe-SEM measurements.

Sample	Thickness (μm)	Porosity (%)
MnCu_850_15	7.6 ± 0.5	24.8
MnCu_875_10	4.3 ± 0.3	21.0
MnCu_900_1	4.8 ± 0.5	22.7

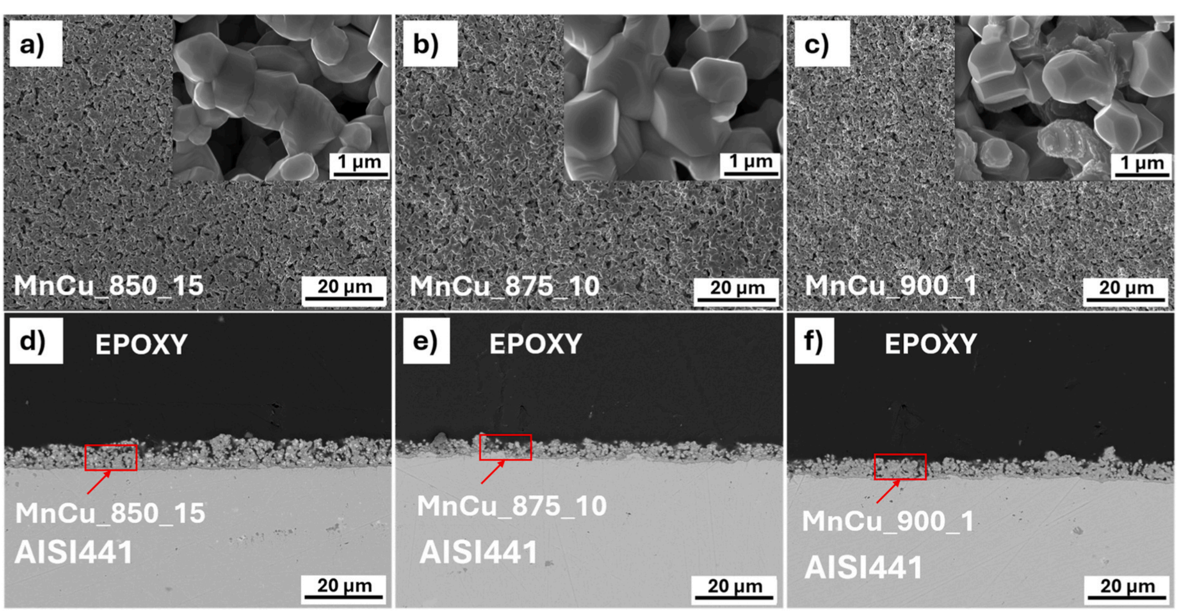

Fig. 5. FE-SEM images of Mn–Cu coatings showing top-view and cross-sectional morphologies for the investigated samples: a) Top-view MnCu_850_15; b) Top-view of MnCu_875_10; c) Top-view of MnCu_900_1; d) Cross-sectional view of MnCu_850_15; e) Cross-sectional view of MnCu_875_10; f) Cross-sectional view of MnCu_900_1.

coating. This morphology is expected to be less detrimental to oxidation protection than interconnected open porosity, since continuous channels do not promote direct oxygen transport toward the substrate. Previous studies on spinel-coated SOC interconnects have shown that even porous spinel coatings can reduce chromium evaporation and contribute to oxidation protection, although denser coatings generally provide improved barrier efficiency [40]. Therefore, the coatings should not be considered fully dense; in this work, densification refers to coating consolidation and interparticle bonding induced by RTP, rather than the formation of fully dense protective layers.

The similar porosity values across all samples indicate that the overall level of densification is comparable, whereas the reduction in thickness with increasing processing severity suggests that densification is accompanied by volumetric shrinkage rather than a significant decrease in total porosity. This behaviour highlights that RTP conditions primarily influence the densification pathway and microstructural evolution rather than the final porosity.

Taken together, the FE-SEM observations and quantitative analysis

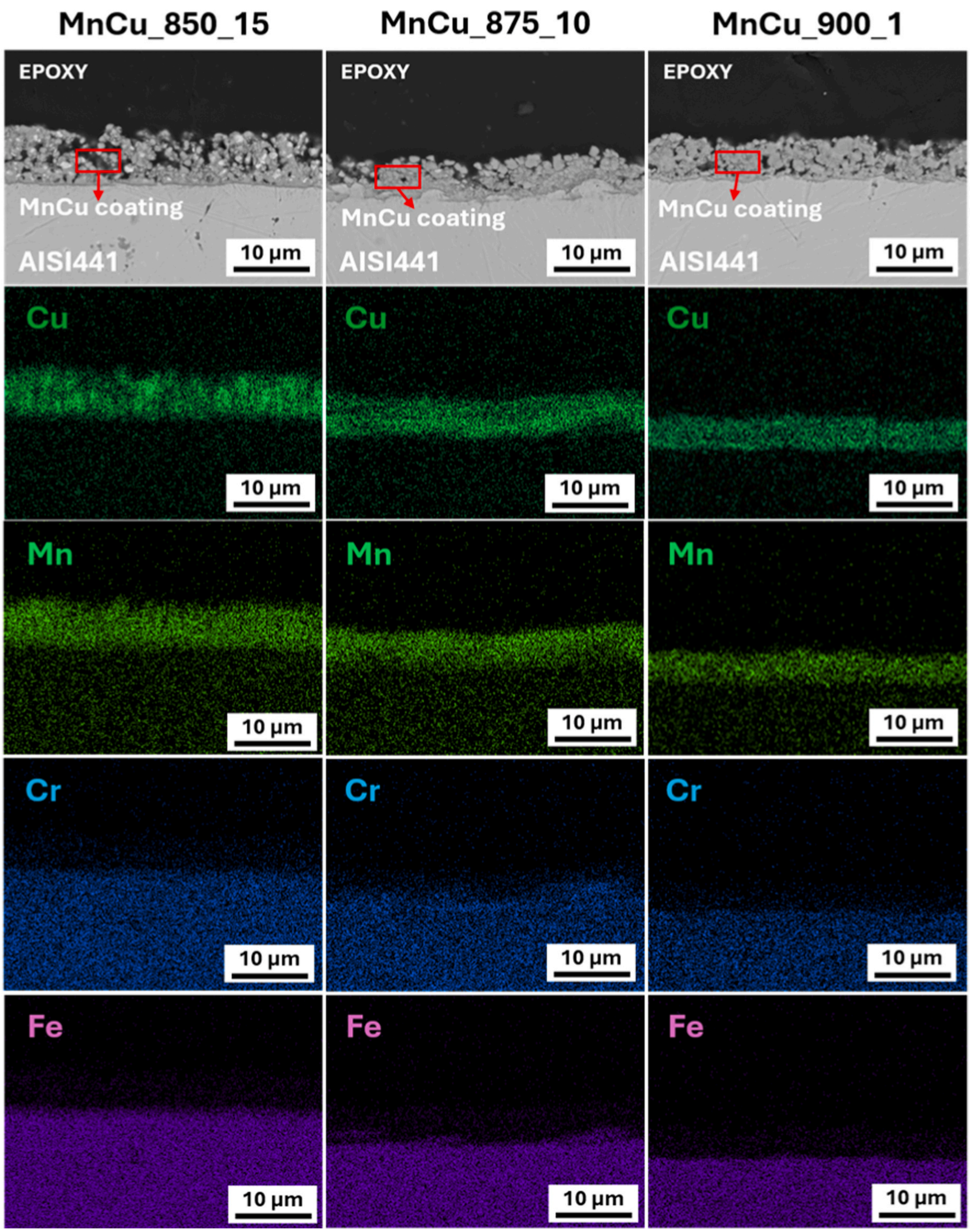

Fig. 6. Cross-sectional FE-SEM images and corresponding EDS elemental maps of MnCu_850_15, MnCu_875_10 and MnCu_900_1 RTP-treated samples.

reveal a trade-off between coating compactness and thickness homogeneity. The MnCu_850_15 coating exhibits lower densification but a more homogeneous thickness distribution, indicating a more uniform consolidation of the deposited layer. In contrast, MnCu_875_10 results in a more compact microstructure despite the shorter dwell time, confirming the strong influence of temperature on densification. However, this improvement in compactness is accompanied by reduced thickness uniformity. The MnCu_900_1 sample exhibits behaviour comparable to MnCu_875_10, indicating that both temperature and dwell time contribute to determining the final coating morphology. This suggests that faster densification at higher temperatures may promote localized shrinkage and particle aggregation, leading to a non-uniform redistribution of material across the coating. Therefore, while higher temperatures and shorter dwell times can enhance coating compactness, they may also reduce coating homogeneity.

It is worth noting that the obtained thickness values are lower than those typically required for protective interconnect coatings (10–20 μm) [2,7,12,74]. However, this limitation is not intrinsic to the RTP approach and can be addressed by optimizing the EPD deposition parameters, for example by increasing the initial coating thickness prior to sintering.

3.5. Elemental distribution

Elemental distribution in the RTP-treated coatings was investigated by cross-sectional EDS mapping, as shown in Fig. 6, to evaluate possible chromium diffusion from the AISI 441 substrate into the coating. The elemental maps confirm that the coatings are primarily composed of Mn and Cu, while chromium remains mainly confined to the substrate. No significant chromium enrichment is detected within the coating or at its surface, and no continuous chromia scale is observed at the coating/substrate interface at the spatial resolution of EDS. This result highlights a key advantage of the proposed RTP-based approach. The absence of detectable chromia enrichment can be related to the reduced thermal exposure associated with rapid thermal cycles, which appears to limit chromium outward diffusion during the coating consolidation step. In conventional thermal treatments, prolonged high-temperature exposure typically promotes the formation of a continuous chromia layer at the interface, which is known to increase electrical resistance and degrade interconnect performance. It should be noted, however, that the absence of a detectable chromia scale after RTP does not imply that chromia formation is completely suppressed during long-term SOC operation. A thin chromia layer may still develop during high-temperature exposure and can contribute to the passivation of the ferritic stainless-steel substrate. However, excessive chromia growth is detrimental as it increases interfacial electrical resistance, particularly at intermediate and lower operating temperatures [55,79]. Therefore, the advantage of RTP lies in limiting chromia scale formation during the coating consolidation step while preserving a spinel-based coating/substrate interface expected to be chemically and thermo-mechanically compatible during subsequent operation. In this context, RTP's ability to limit detectable chromium diffusion and chromia scale development is a significant advantage, as it may improve interfacial stability while reducing degradation associated with excessive oxide-scale growth. Nevertheless, long-term oxidation and electrochemical testing will be required to confirm the stability and protective behaviour of the coating/substrate interface under realistic SOC operating conditions.

4. Discussion

The combined results obtained from HT-XRD, XRD, FE-SEM, porosity/thickness analysis, and EDS mapping allow the investigated RTP conditions to be assessed beyond visual inspection of coating integrity. The HT-XRD analysis identified 950 °C as a critical temperature region for Mn–Cu spinel phase evolution under prolonged thermal exposure, while the processing window confirmed that treatments at this temperature lead to cracking and/or delamination. This indicates that, although RTP strongly reduces the duration of thermal exposure, excessive peak temperatures can still negatively affect coating integrity, likely due to transient phase evolution and thermo-mechanical stress development during heating. At the opposite side of the processing window, 800 °C was insufficient to promote adequate coating consolidation and adhesion, even with a longer dwell time. This confirms that a minimum thermal input is required to activate sintering and interparticle bonding. Therefore, the effective RTP window is defined by a balance between insufficient densification at low temperature and excessive thermal stress or phase evolution at high temperature.

Among the defect-free coatings, MnCu_850_15 exhibited the most homogeneous thickness distribution but also showed a less compact microstructure and a more pronounced CuO-related contribution. This suggests that longer dwell times may favour copper redistribution and secondary phase evolution, even at comparatively lower temperatures. In contrast, MnCu_900_1 enabled rapid densification within only 1 min, but the resulting coating showed reduced thickness homogeneity and less uniform microstructural development, likely due to localized shrinkage during fast densification. MnCu_875_10 therefore represents the most balanced condition among those investigated, combining good adhesion, crack-free morphology, compact microstructure, limited CuO-related phase evolution, and significantly reduced processing time. These results indicate that the most suitable RTP processing range for Mn–Cu spinel coatings lies between 850 and 900 °C with short dwell times, with 875 °C for 10 min providing the best compromise between densification, coating uniformity, phase composition, and reduced thermal exposure.

The EDS results further support the relevance of RTP for interconnect coating fabrication, as no detectable chromia scale formation or chromium enrichment was observed at the coating/substrate interface after thermal treatment. This result should not be interpreted as the complete suppression of chromia formation during SOC operation. Rather, it indicates that RTP can limit excessive oxide-scale growth during the coating consolidation step. This aspect is particularly important because, although a thin chromia layer can contribute to steel passivation and coating adhesion [8,79,80], excessive chromia growth increases interfacial resistance and may become especially detrimental at reduced SOC operating temperatures [55,78]. During long-term operation, a thin oxide scale may still form at the interface; however, the selected Mn–Cu spinel coating is expected to mitigate further outward diffusion of chromium and maintain chemical and thermo-mechanical compatibility with the ferritic substrate. Long-term oxidation and electrochemical testing will be required to confirm this behaviour under realistic operating conditions.

Nonetheless, the relatively low coating thickness and residual porosity obtained in this work remain important limitations. Although the coatings are continuous, adherent, and crack-free, they should not yet be considered fully optimized protective layers for long-term SOC operation. The present study should therefore be regarded as a proof of concept demonstrating the feasibility of RTP-assisted sintering of EPD-derived Mn–Cu spinel coatings under reduced thermal exposure. Nevertheless, cross-sectional SEM observations suggest that the residual porosity is mainly isolated/closed rather than forming continuous open pathways through the coating. Moreover, a relatively compact region can be observed close to the coating/substrate interface, which may still contribute to limiting direct oxygen transport toward the substrate. Previous studies on spinel-coated interconnects have shown that even porous coatings can reduce oxidation and chromium evaporation, although denser and thicker coatings generally provide improved barrier efficiency [11,40].

Future work will focus on optimizing the EPD deposition step to increase coating thickness and reduce residual porosity, for example by increasing the deposited mass or by exploring multi-step deposition strategies. Long-term oxidation and electrochemical tests under SOC-relevant conditions will then be required to validate the protective performance of the optimized coatings.

Overall, the results demonstrate that RTP is not simply a faster alternative to conventional sintering, but a processing route in which temperature and dwell time must be carefully balanced to control densification, phase evolution, coating uniformity, and interfacial stability.

5. Conclusions

Compact Mn–Cu spinel coatings were successfully fabricated on AISI 441 ferritic stainless steel by combining EPD and RTP. The process enabled partially densified and crack-free coatings in less than 1 h, confirming RTP as an effective route to reduce the thermal budget of EPD-derived protective coatings.

HT-XRD identified 950 °C as a critical temperature region for Mn–Cu spinel phase evolution, while RTP experiments showed that excessive peak temperatures lead to cracking and/or delamination. Among the investigated conditions, 875 °C for 10 min provided the best compromise between coating densification, thickness uniformity, phase composition, and reduced processing time. EDS mapping showed no detectable chromia scale formation or chromium enrichment at the coating/substrate interface after RTP treatment, highlighting the potential of the approach to limit interfacial degradation during processing. Although the coatings obtained in this work are not yet fully optimized in terms of thickness and residual porosity, the results demonstrate that RTP-assisted EPD is a promising strategy for the rapid fabrication of Mn–Cu spinel coatings for SOC interconnect applications. Further optimization of the EPD step and long-term oxidation/electrochemical testing will be required to fully assess their protective performance under realistic SOC operating conditions.

CRediT authorship contribution statement

Francesco Gallo: Conceptualization, Formal analysis, Investigation, Visualization, Writing – original draft, Writing – review & editing. **Marc Torrell:** Conceptualization, Supervision. **Lucile Bernadet:** Conceptualization, Supervision, Writing – review & editing. **Simone Anelli:** Conceptualization, Supervision, Writing – review & editing. **Fabiana D'Isanto:** Conceptualization, Supervision, Writing – review & editing. **Dario Montinaro:** Resources. **Federico Smeacetto:** Conceptualization, Supervision, Writing – review & editing.

Declaration of generative AI and AI-assisted technologies in the writing process

During the preparation of this work the author(s) used ChatGPT (OpenAI) to improve the readability and language of the manuscript. After using this tool/service, the author(s) reviewed and edited the content as needed and take(s) full responsibility for the content of the publication.

Declaration of competing interests

The authors declare that they have no known competing financial interests or personal relationships that could have appeared to influence the work reported in this paper.

Acknowledgements

This research has been funded by the European Union GA No. 101101418 (24_7 ZEN project). Views and opinions expressed are, however, those of the author(s) only and do not necessarily reflect those of the European Union or Clean Hydrogen Joint Undertaking. Neither the European Union nor the granting authority can be held responsible for them.

References

[1] W.J. Quadakkers, J. Prion-Abellan, V. Shemet, L. Singheiser, Metallic interconnectors for solid oxide fuel cells – a review, Mater. A. T. High. Temp. 20 (2003) 115–127.

[2] J.C.W. Mah, A. Muchtar, M.R. Somalu, M.J. Ghazali, Metallic interconnects for solid oxide fuel cell: a review on protective coating and deposition techniques, Int. J. Hydrogen Energy 42 (2017) 9219–9229, https://doi.org/10.1016/j.ijhydene.2016.03.195.

[3] R. Scataglini, M. Wei, A. Mayyas, S.H. Chan, T. Lipman, M. Santarelli, A direct manufacturing cost model for solid-oxide fuel cell stacks, Fuel Cells 17 (2017) 825–842, https://doi.org/10.1002/fuce.201700012.

[4] N. Shaigan, W. Qu, D.G. Ivey, W. Chen, A review of recent progress in coatings, surface modifications and alloy developments for solid oxide fuel cell ferritic stainless steel interconnects, J. Power Sources 195 (2010) 1529–1542, https://doi.org/10.1016/j.jpowsour.2009.09.069.

[5] Y. Hao, R. Zhu, H. Cao, Z. Liu, R. Ran, G. Yang, A mini-review on mitigating degradation of metallic interconnects in solid oxide cell stack systems: advances, challenges, and solutions, Energy Fuels 39 (2025) 18751–18772, https://doi.org/10.1021/acs.energyfuels.5c03611.

[6] Y. Hu, D. Li, H. Guo, S.H. Liu, Y. Meng, S. Ding, C.X. Li, Recent progress of high-performance interconnectors for SOFC: from materials, protective coatings, optimizing strategies, towards the real stack applications, Chem. Eng. J. 505 (2025), https://doi.org/10.1016/j.cej.2025.159321.

[7] T. Horita, H. Kishimoto, K. Yamaji, Y. Xiong, N. Sakai, M.E. Brito, H. Yokokawa, Evaluation of Laves-phase forming Fe-Cr alloy for SOFC interconnects in reducing atmosphere, J. Power Sources 176 (2008) 54–61, https://doi.org/10.1016/j.jpowsour.2007.10.041.

[8] H. Falk-Windisch, J.E. Svensson, J. Froitzheim, The effect of temperature on chromium vaporization and oxide scale growth on interconnect steels for solid oxide Fuel Cells, J. Power Sources 287 (2015) 25–35, https://doi.org/10.1016/j.jpowsour.2015.04.040.

[9] M.T. Mehran, M.Z. Khan, R.H. Song, T.H. Lim, M. Naqvi, R. Raza, B. Zhu, M. B. Hanif, A comprehensive review on durability improvement of solid oxide fuel cells for commercial stationary power generation systems, Appl. Energy 352 (2023), https://doi.org/10.1016/j.apenergy.2023.121864.

[10] S.P. Jiang, X. Chen, Chromium deposition and poisoning of cathodes of solid oxide fuel cells - a review, Int. J. Hydrogen Energy 39 (2014) 505–531, https://doi.org/10.1016/j.ijhydene.2013.10.042.

[11] M.J. Reddy, B. Kamecki, B. Talic, E. Zanchi, F. Smeacetto, J.S. Hardy, J.P. Choi, Ł. Mazur, R. Vaßen, S.N. Basu, T. Brylewski, J.-E. Svensson, J. Froitzheim, Experimental review of the performances of protective coatings for interconnects in solid oxide fuel cells, J. Power Sources 568 (2023) 232831, https://doi.org/10.1016/j.jpowsour.2023.232831.

[12] M. Stanislowski, J. Froitzheim, L. Niewolak, W.J. Quadakkers, K. Hilpert, T. Markus, L. Singheiser, Reduction of chromium vaporization from SOFC interconnectors by highly effective coatings, J. Power Sources 164 (2007) 578–589, https://doi.org/10.1016/j.jpowsour.2006.08.013.

[13] Z. Yang, G.G. Xia, X.H. Li, J.W. Stevenson, Mn,Co)3O4 spinel coatings on ferritic stainless steels for SOFC interconnect applications, Int. J. Hydrogen Energy 32 (2007) 3648–3654, https://doi.org/10.1016/j.ijhydene.2006.08.048.

[14] J. Mao, E. Wang, H. Wang, M. Ouyang, Y. Chen, H. Hu, L. Lu, D. Ren, Y. Liu, Progress in metal corrosion mechanism and protective coating technology for interconnect and metal support of solid oxide cells, Renew. Sustain. Energy Rev. 185 (2023), https://doi.org/10.1016/j.rser.2023.113597.

[15] T.N. Myasoedova, R. Kalusulingam, T.S. Mikhailova, Sol-gel materials for electrochemical applications: recent advances, Coatings 12 (2022), https://doi.org/10.3390/coatings12111625.

[16] H. Shi, H. Li, X. Zhou, C. Yang, H. Tu, J. Tong, L. Xiang, C. Ma, L. Zhu, Z. Huang, Effects of transition metals on the electrical conductivity of M-Doped MnCo2O4 (M = Cu, Ni, Zn) as contact layer on precoated SUS441 in solid oxide cells, ACS Appl. Energy Mater. 7 (2024) 2542–2551, https://doi.org/10.1021/acsaem.4c00207.

[17] A. Runts, G. Bleykher, S. Stepanov, D. Valiev, Reactive magnetron deposition of YAG:Ce phosphor coatings in the metallic mode, Opt. Mater. 156 (2024), https://doi.org/10.1016/j.optmat.2024.115946.

[18] F. Buzi, L. Bernadet, J. Orrit-Prat, R. Bonet, J. Caro, D. Montinaro, J.P. Ouweltjes, F. Baiutti, M. Torrell, A. Morata, A. Tarancón, Advanced manufacturing for efficient GDC diffusion barrier layer by rapid thermal processing for large-area solid oxide cells, J. Power Sources 652 (2025), https://doi.org/10.1016/j.jpowsour.2025.237629.

[19] Z. Zakaria, Z. Awang Mat, S.H. Abu Hassan, Y. Boon Kar, A review of solid oxide fuel cell component fabrication methods toward lowering temperature, Int. J. Energy Res. 44 (2020) 594–611, https://doi.org/10.1002/er.4907.

[20] O.O. Abegunde, E.T. Akinlabi, O.P. Oladijo, S. Akinlabi, A.U. Ude, Overview of thin film deposition techniques, AIMS Mater. Sci. 6 (2019) 174–199, https://doi.org/10.3934/MATERSCI.2019.2.174.

[21] L. Bernadet, J. Segura-Ruiz, L. Yedra, S. Estrade, F. Peiró, D. Montinaro, M. Torrell, A. Morata, A. Tarancón, Enhanced diffusion barrier layers for avoiding degradation in SOFCs aged for 14000 h during 2 years, J. Power Sources 555 (2023), https://doi.org/10.1016/j.jpowsour.2022.232400.

[22] N.S. Waluyo, S.S. Park, R.H. Song, S.B. Lee, T.H. Lim, J.E. Hong, K.H. Ryu, W. Bin Im, J.W. Lee, Protective coating based on manganese–copper oxide for solid oxide fuel cell interconnects: plasma spray coating and performance evaluation, Ceram. Int. 44 (2018) 11576–11581, https://doi.org/10.1016/j.ceramint.2018.03.220.

[23] R. Spotorno, P. Piccardo, F. Perrozzi, S. Valente, M. Viviani, A. Ansar, Microstructural and electrical characterization of plasma sprayed Cu-Mn oxide

spinels as coating on metallic interconnects for stacking solid oxide fuel cells, Fuel Cells (2015) 728–734, https://doi.org/10.1002/fuce.201400189. John Wiley and Sons Ltd.

[24] M. Cannio, S. Novak, L. Besra, A.R. Boccaccini, Electrophoretic deposition, in: Ceramics and Composites Processing Methods, Wiley, 2012, pp. 517–549, https://doi.org/10.1002/9781118176665.ch15.

[25] L. Besra, M. Liu, A review on fundamentals and applications of electrophoretic deposition (EPD), Prog. Mater. Sci. 52 (2007) 1–61, https://doi.org/10.1016/j.pmatsci.2006.07.001.

[26] P. Amrollahi, J.S. Krasinski, R. Vaidyanathan, L. Tayebi, D. Vashaee, Electrophoretic deposition (EPD): fundamentals and applications from Nano- to micro-scale structures, in: Handbook of Nanoelectrochemistry, Springer International Publishing, 2015, pp. 1–27, https://doi.org/10.1007/978-3-319-15207-3_7-1.

[27] P. Sarkar, D. De, H. Rho, Synthesis and microstructural manipulation of ceramics by electrophoretic deposition, J. Mater. Sci. 39 (2004) 819–823, https://doi.org/10.1023/B:JMSC.0000012909.46419.0e.

[28] S. Hu, W. Li, H. Finklea, X. Liu, A review of electrophoretic deposition of metal oxides and its application in solid oxide fuel cells, Adv. Colloid Interface Sci. 276 (2020), https://doi.org/10.1016/j.cis.2020.102102.

[29] M. Hilger, K. El Jardali, V. Feyzi, D. Vakhrameev, D. Naumenko, R. Schwaiger, D. Iribarren, C. Lenser, O. Guillon, N.H. Menzler, Towards sustainable interconnects for solid oxide cells: an integrated technical and environmental evaluation of coating methods, J. Power Sources 659 (2025), https://doi.org/10.1016/j.jpowsour.2025.238471.

[30] H. Sa'adati, B. Raissi, R. Riahifar, M.S. Yaghmaee, How preparation of suspensions affects the electrophoretic deposition phenomenon, J. Eur. Ceram. Soc. 36 (2016) 299–305, https://doi.org/10.1016/j.jeurceramsoc.2015.09.005.

[31] B. Ferrari, R. Moreno, EPD kinetics: a review, J. Eur. Ceram. Soc. 30 (2010) 1069–1078, https://doi.org/10.1016/j.jeurceramsoc.2009.08.022.

[32] M. Bobruk, S. Molin, M. Chen, T. Brylewski, P.V. Hendriksen, Sintering of MnCo2O4 coatings prepared by electrophoretic deposition, Mater. Lett. 213 (2018) 394–398, https://doi.org/10.1016/j.matlet.2017.12.046.

[33] F. Smeacetto, A. De Miranda, S. Cabanas Polo, S. Molin, D. Boccaccini, M. Salvo, A. R. Boccaccini, Electrophoretic deposition of Mn1.5Co1.5O4 on metallic interconnect and interaction with glass-ceramic sealant for solid oxide fuel cells application, J. Power Sources 280 (2015) 379–386, https://doi.org/10.1016/j.jpowsour.2015.01.120.

[34] O. Ekhlasiosgouei, F. Smeacetto, S. Molin, Suspension and process parameters selection for electrophoretic deposition of Mn–Co spinel coating on steel interconnects, Int. J. Hydrogen Energy 60 (2024) 1054–1067, https://doi.org/10.1016/j.ijhydene.2024.02.252.

[35] A.G. Sabato, S. Molin, H. Javed, E. Zanchi, A.R. Boccaccini, F. Smeacetto, In-situ Cu-doped MnCo-spinel coatings for solid oxide cell interconnects processed by electrophoretic deposition, Ceram. Int. 45 (2019) 19148–19157, https://doi.org/10.1016/j.ceramint.2019.06.161.

[36] E. Zanchi, S. Molin, A.G. Sabato, B. Talic, G. Cempura, A.R. Boccaccini, F. Smeacetto, Iron doped manganese cobaltite spinel coatings produced by electrophoretic co-deposition on interconnects for solid oxide cells: microstructural and electrical characterization, J. Power Sources 455 (2020), https://doi.org/10.1016/j.jpowsour.2020.227910.

[37] E. Zanchi, B. Talic, A.G. Sabato, S. Molin, A.R. Boccaccini, F. Smeacetto, Electrophoretic co-deposition of Fe2O3 and Mn1,5Co1,5O4: processing and oxidation performance of Fe-doped Mn-Co coatings for solid oxide cell interconnects, J. Eur. Ceram. Soc. 39 (2019) 3768–3777, https://doi.org/10.1016/j.jeurceramsoc.2019.05.024.

[38] B. Talic, P.V. Hendriksen, K. Wiik, H.L. Lein, Thermal expansion and electrical conductivity of Fe and Cu doped MnCo2O4 spinel, Solid State Ionics 326 (2018) 90–99, https://doi.org/10.1016/j.ssi.2018.09.018.

[39] B. Talic, V. Venkatachalam, P.V. Hendriksen, R. Kiebach, Comparison of MnCo2O4 coated Crofer 22 H, 441, 430 as interconnects for intermediate-temperature solid oxide fuel cell stacks, J. Alloys Compd. 821 (2020), https://doi.org/10.1016/j.jallcom.2019.153229.

[40] B. Talic, H. Falk-Windisch, V. Venkatachalam, P.V. Hendriksen, K. Wiik, H.L. Lein, Effect of coating density on oxidation resistance and Cr vaporization from solid oxide fuel cell interconnects, J. Power Sources 354 (2017) 57–67, https://doi.org/10.1016/j.jpowsour.2017.04.023.

[41] E. Zanchi, J. Ignaczak, S. Molin, G. Cempura, A.R. Boccaccini, F. Smeacetto, Electrophoretic co-deposition of Mn1.5Co1.5O4, Fe2O3 and CuO: unravelling the effect of simultaneous addition of Cu and Fe on the microstructural, thermo-mechanical and corrosion properties of in-situ modified spinel coatings for solid oxide cell interconnects, J. Eur. Ceram. Soc. 42 (2022) 3271–3281, https://doi.org/10.1016/j.jeurceramsoc.2022.02.008.

[42] F.W. Schwartz, S. Lee, T.H. Darrah, A review of the scope of artisanal and small-scale mining worldwide, poverty, and the associated health impacts, GeoHealth 5 (2021), https://doi.org/10.1029/2020GH000325.

[43] L. Leyssens, B. Vinck, C. Van Der Straeten, F. Wuyts, L. Maes, Cobalt toxicity in humans—A review of the potential sources and systemic health effects, Toxicology 387 (2017) 43–56, https://doi.org/10.1016/j.tox.2017.05.015.

[44] J. Ignaczak, M. Bik, J. Jamroz, K. Górnicka, A. Drewniak, J. Karczewski, P. Jasiński, S. Molin, Development and evaluation of interconnect protective coatings based on commercial Mn1.9CuFe0.1O4 spinel powder, J. Eur. Ceram. Soc. 45 (2025), https://doi.org/10.1016/j.jeurceramsoc.2025.117259.

[45] Z. Sun, S. Gopalan, U.B. Pal, S.N. Basu, Cu1.3Mn1.7O4 spinel coatings deposited by electrophoretic deposition on Crofer 22 APU substrates for solid oxide fuel cell applications, Surf. Coat. Technol. 323 (2017) 49–57, https://doi.org/10.1016/j.surfcoat.2016.09.028.

[46] Z. Ranjbar-Nouri, M. Soltanieh, S. Rastegari, Applying the protective CuMn2O4 spinel coating on AISI-430 ferritic stainless steel used as solid oxide fuel cell interconnects, Surf. Coat. Technol. 334 (2018) 365–372, https://doi.org/10.1016/j.surfcoat.2017.11.036.

[47] Ł. Mazur, K. Domaradzki, P. Winiarski, M. Bik, A. Mikuła, J. Dąbrowa, G. Cempura, A. Adamczyk, A. Kruk, T. Brylewski, Advanced characterization and functional evaluation of Ni-/Fe-doped Cu-Mn spinels as Co-free coatings for SOFC/SOEC interconnects, J. Mater. Chem. A Mater 13 (2025) 32741–32764, https://doi.org/10.1039/d5ta04138d.

[48] E. Zanchi, A.G. Sabato, S. Molin, G. Cempura, A.R. Boccaccini, F. Smeacetto, Recent advances on spinel-based protective coatings for solid oxide cell metallic interconnects produced by electrophoretic deposition, Mater. Lett. 286 (2021), https://doi.org/10.1016/j.matlet.2020.129229.

[49] Z. Zhu, C. Darl-Uzu, U. Pal, S. Gopalan, A.M. Hussain, N. Dale, Y. Fukuyama, Y. Miura, Y. Miyoshi, S. Basu, Comparison of Cu–Mn and Mn–Co spinel coatings for solid oxide fuel cell interconnects, Int. J. Hydrogen Energy 47 (2022) 36953–36963, https://doi.org/10.1016/j.ijhydene.2022.08.239.

[50] S. Joshi, A. Petric, Nickel substituted CuMn2O4 spinel coatings for solid oxide fuel cell interconnects, Int. J. Hydrogen Energy 42 (2017) 5584–5589, https://doi.org/10.1016/j.ijhydene.2016.08.075.

[51] J. Ignaczak, Y. Naumovich, K. Górnicka, J. Jamroz, W. Wróbel, J. Karczewski, M. Chen, P. Jasiński, S. Molin, Preparation and characterisation of iron substituted Mn1.7Cu1.3-xFexO4 spinel oxides (x = 0, 0.1, 0.3, 0.5), J. Eur. Ceram. Soc. 40 (2020) 5920–5929, https://doi.org/10.1016/j.jeurceramsoc.2020.07.001.

[52] A. Petric, H. Ling, Electrical conductivity and thermal expansion of spinels at elevated temperatures, J. Am. Ceram. Soc. 90 (2007) 1515–1520, https://doi.org/10.1111/j.1551-2916.2007.01522.x.

[53] Ł. Mazur, K. Domaradzki, P. Winiarski, Ł. Zych, T. Brylewski, Optimization of electrophoretic deposition and thermal treatment of Cu–Mn spinel matrix for spinel/perovskite composite coating used as SOC metallic interconnect, Ceram. Int. 50 (2024) 34017–34026, https://doi.org/10.1016/j.ceramint.2024.06.221.

[54] O. Ekhlasiosgouei, Oxidation, electrical and thermal properties of spinel protective coating by EPD method for SOFCs application: a comprehensive review, Int. J. Hydrogen Energy 197 (2026), https://doi.org/10.1016/j.ijhydene.2025.152649.

[55] K. Wang, Y. Liu, J.W. Fergus, Interactions between SOFC interconnect coating materials and chromia, J. Am. Ceram. Soc. 94 (2011) 4490–4495, https://doi.org/10.1111/j.1551-2916.2011.04749.x.

[56] B. Yoon, V. Avila, I.R. Lavagnini, J.V. Campos, L.M. Jesus, Reactive flash sintering of ceramics: a review, Adv. Eng. Mater. 25 (2023), https://doi.org/10.1002/adem.202200731.

[57] K.S. Naik, V.M. Sglavo, R. Raj, Field assisted sintering of ceramic constituted by alumina and yttria stabilized zirconia, J. Eur. Ceram. Soc. 34 (2014) 2435–2442, https://doi.org/10.1016/j.jeurceramsoc.2014.02.042.

[58] J. Langer, D.V. Quach, J.R. Groza, O. Guillon, A comparison between fast and sps apparatuses based on the sintering of oxide ceramics, Int. J. Appl. Ceram. Technol. 8 (2011) 1459–1467, https://doi.org/10.1111/j.1744-7402.2010.02604.x.

[59] R.I. Todd, Flash sintering of ceramics: a short review, in: Proceedings of the IV Advanced Ceramics and Applications Conference, Atlantis Press, 2017, pp. 1–12, https://doi.org/10.2991/978-94-6239-213-7_1.

[60] V.G. Karayannis, Microwave sintering of ceramic materials, IOP Conf. Ser. Mater. Sci. Eng. 161 (2016) 012068, https://doi.org/10.1088/1757-899X/161/1/012068.

[61] R.X. Luo, M. Kermani, Z.L. Guo, J. Dong, C.F. Hu, F. Zuo, S. Grasso, B.B. Jiang, G. L. Nie, Z.Q. Yan, Q. Wang, Y.L. Gan, F.P. He, H.T. Lin, Ultrafast high-temperature sintering of silicon nitride: a comparison with the state-of-the-art techniques, J. Eur. Ceram. Soc. 41 (2021) 6338–6345, https://doi.org/10.1016/j.jeurceramsoc.2021.06.021.

[62] L. Porz, M. Scherer, D. Huhn, L.M. Heine, S. Britten, L. Rebohle, M. Neubert, M. Brown, P. Lascelles, R. Kitson, D. Rettenwander, L. Fulanovic, E. Bruder, P. Breckner, D. Isaia, T. Frömling, J. Rödel, W. Rheinheimer, Blacklight sintering of ceramics, Mater. Horiz. 9 (2022) 1717–1726, https://doi.org/10.1039/d2mh00177b.

[63] W.S. Scheld, S. Lobe, C. Dellen, M. Ihrig, G. Häuschen, L.C. Hoff, M. Finsterbusch, S. Uhlenbruck, O. Guillon, D. Fattakhova-Rohlfing, Rapid thermal processing of garnet-based composite cathodes, J. Power Sources 545 (2022), https://doi.org/10.1016/j.jpowsour.2022.231872.

[64] S.R. Wilson, R.B. Gregory, W.M. Paulson, An overview and comparison of rapid thermal processing equipment: a users viewpoint, MRS Proceedings 52 (1985) 181, https://doi.org/10.1557/PROC-52-181.

[65] C. Yuan, L. Zhang, W. Liu, C. Zhu, Rapid thermal process to fabricate Sb2Se3 thin film for solar cell application, Sol. Energy 137 (2016) 256–260, https://doi.org/10.1016/j.solener.2016.08.020.

[66] M.A. Olğar, Y. Atasoy, Preparation of czts thin film employing rapid thermal processing method, Eurasian Journal of Science Engineering and Technology 3 (2022) 29–35, https://doi.org/10.55696/ejset.1098850.

[67] Thyssenkrupp, Stainless steel 441 1.4509 safety data sheet. https://www.thyssenkrupp-materials.co.uk/stainless-steel-441-14509.html10_04_2026. (Accessed 10 April 2026). https://d2zo35mdb530wx.cloudfront.net/_legacy/UCPthyssenkruppBAMXUK/assets.files/material-data-sheets/stainless-steel/stainless-steel-1.4509-441.pdf.

[68] S.U. Oh, D. Kim, I.T. Lee, C.S. Choi, J.A. Lee, Y.W. Heo, J.H. Lee, Electrophoretic deposition and low-temperature densification of Cu1.35Mn1.65O4 spinel for an interconnect protective coating in solid oxide fuel cells, Int. J. Hydrogen Energy 47 (2022) 33410–33419, https://doi.org/10.1016/j.ijhydene.2022.07.259.

[69] J. Ignaczak, L. Zeng, D.F. Sanchez, M. Makowska, K. Górnicka, K. Lankauf, J. Karczewski, P. Jasiński, S. Molin, Fe-modified Mn2CuO4 spinel oxides: coatings based on abundant elements for solid oxide cell interconnects, Int. J. Hydrogen Energy (2023), https://doi.org/10.1016/j.ijhydene.2023.06.041.

[70] R.E. Vandenberghe, G.G. Robbrecht, V.A.M. Brabers, On the stability of the cubic spinel structure in the system cu\uff00mn\ue5f8o, es. Bull. 8 (1973) 571–579, https://doi.org/10.1016/0025-5408(73)90134-7.

[71] W. Qu, L. Jian, J.M. Hill, D.G. Ivey, Electrical and microstructural characterization of spinel phases as potential coatings for SOFC metallic interconnects, J. Power Sources 153 (2006) 114–124, https://doi.org/10.1016/j.jpowsour.2005.03.137.

[72] Ł. Mazur, S. Molin, J. Dąbek, K. Durczak, M. Pyzalski, T. Brylewski, Physicochemical properties of Mn1.45Co1.45Cu0.1O4 spinel coating deposited on the crofer 22 H ferritic steel and exposed to high-temperature oxidation under thermal cycling conditions, J. Therm. Anal. Calorim. 147 (2022) 5649–5666, https://doi.org/10.1007/s10973-021-10884-2.

[73] S. Molin, A.G. Sabato, M. Bindi, P. Leone, G. Cempura, M. Salvo, S. Cabanas Polo, A.R. Boccaccini, F. Smeacetto, Microstructural and electrical characterization of Mn-Co spinel protective coatings for solid oxide cell interconnects, J. Eur. Ceram. Soc. 37 (2017) 4781–4791, https://doi.org/10.1016/j.jeurceramsoc.2017.07.011.

[74] W.Q. Qiao, Y.W. Li, Y.S. Zhang, M.H. Wang, K. Li, Z.J. Li, W. Yang, Cu- and Ce-doped MnCo2O4 spinel coatings on ferrite interconnects by electrophoretic deposition, Mater. Today Commun. 38 (2024), https://doi.org/10.1016/j.mtcomm.2024.108061.

[75] R. Wang, Z. Sun, U.B. Pal, S. Gopalan, S.N. Basu, Mitigation of chromium poisoning of cathodes in solid oxide fuel cells employing CuMn1.8O4 spinel coating on metallic interconnect, J. Power Sources 376 (2018) 100–110, https://doi.org/10.1016/j.jpowsour.2017.11.069.

[76] T. Brylewski, S. Molin, M. Marczyński, Mazur, K. Domaradzki, O. Kryshtal, A. Gil, Influence of Gd deposition on the oxidation behavior and electrical properties of a layered system consisting of Crofer 22 APU and MnCo2O4 spinel, Int. J. Hydrogen Energy 46 (2021) 6775–6791, https://doi.org/10.1016/j.ijhydene.2020.11.169.

[77] Ł. Mazur, J. Ignaczak, M. Bik, S. Molin, M. Sitarz, Aleksander Gil, T. Brylewski, Effectiveness of a dual surface modification of metallic interconnects for application in energy conversion devices, Int. J. Hydrogen Energy 47 (2022) 6295–6311, https://doi.org/10.1016/j.ijhydene.2021.11.256.

[78] S. Fontana, R. Amendola, S. Chevalier, P. Piccardo, G. Caboche, M. Viviani, R. Molins, M. Sennour, Metallic interconnects for SOFC: characterisation of corrosion resistance and conductivity evaluation at operating temperature of differently coated alloys, J. Power Sources 171 (2007) 652–662, https://doi.org/10.1016/j.jpowsour.2007.06.255.

[79] A. Holt, P. Kofstad, Electrical conductivity and defect structure of Cr2O3. II. Reduced temperatures ($<\sim 1000^{\circ}$C), Solid State Ionics 69 (1994) 137–143, https://doi.org/10.1016/0167-2738(94)90402-2.

[80] J. Mikkola, K. Couturier, B. Talic, S. Frangini, N. Giacometti, N. Pelissier, B. R. Sudireddy, O. Thomann, Protective coatings for ferritic stainless steel interconnect materials in high temperature solid oxide electrolyser atmospheres, Energies 15 (2022), https://doi.org/10.3390/en15031168 (Basel).